

Selective-Resputtering-Induced Perpendicular Magnetic Anisotropy in Amorphous TbFe Films

Vincent G. Harris¹ and Taras Pokhil²

¹Naval Research Laboratory, Washington, D.C. 20375-5000

²Seagate Technology, Minneapolis, Minnesota 55435-5489

(Received 7 March 2001; published 23 July 2001)

Perpendicular magnetic anisotropy energy in rf magnetron sputtered amorphous TbFe films is measured to increase exponentially with pair-order anisotropy induced by the selective resputtering of surface adatoms during film growth.

DOI: 10.1103/PhysRevLett.87.067207

PACS numbers: 75.30.Gw, 61.10.Ht, 75.50.Kj

Since the development in the mid-1960s of sputter-deposition film growth technologies, and their subsequent application to magnetic film processing, growth-induced magnetic anisotropy has often been a natural and yet poorly understood consequence. In crystalline films, where magnetic anisotropy arises predominantly from magnetocrystalline interactions [1], some form of crystal texturing is often responsible. Alternative sources of magnetic anisotropy include columnar growth [2], anisotropic void networks [3], chemical short range order [4,5], and anisotropic stress fields [6,7]. These provide magnetic anisotropy from dipole-dipole (or pseudodipolar) interactions [8] and magnetoelastic interactions [1] (i.e., magnetostriction), respectively. All of these mechanisms are subject to alteration by varying processing conditions. Paradoxically, some amorphous alloys consisting of rare earth and transition metals (a-RETM) display strong growth-induced magnetic anisotropy [9] yet do not show signs of crystalline order, anisotropic morphologies, or other characteristics that might explain its origins [10]. In this Letter, we address the long-standing issue of identifying the growth mechanism responsible for the magnetic anisotropy in sputter-deposited a-RETM films.

Growth-induced magnetic anisotropy in a-RETM films was first discussed by Gambino *et al.* [11] in 1973, shortly following the discovery of perpendicular magnetic anisotropy (PMA) in a-GdCo films [12]. These authors [11] proposed a selective resputtering mechanism to account for a pair order anisotropy (POA) that they believed was responsible for the PMA via the van Vleck pair model [8]. In an extension of this work that further supported the selective resputtering mechanism, a strong correlation was measured between substrate voltage bias and magnetic anisotropy in rf magnetron sputtered a-GdCo films [13]. They envisioned this POA as a statistical preference of Co-Co and Gd-Gd pairs parallel to the film plane and Gd-Co pairs perpendicular to the film plane. However, because of the lack of direct evidence supporting the existence of a POA, selective resputtering was not readily accepted as a growth mechanism leading to PMA.

In the late 1980s, advances in extended x-ray absorption fine structure (EXAFS) theory [14,15] and detector technology [16] allowed Harris *et al.* [17] in 1992 to measure an atomic-scale structural anisotropy (ASA) in

a-TbFe films. The ASA, described as a statistical preference for like atom pairs along the in-plane direction and unlike atom pairs perpendicular to the film plane [17], was shown to correlate strongly with PMA. This description is similar to the POA proposed by Gambino *et al.* [11,13]. An anisotropic local structure is one mechanism that can break the symmetry of the electrostatic environment acting on the RE ion and result in a large magnetic anisotropy via a crystal field interaction. This is the foundation of the single-ion anisotropy model [18]. In a-TbFe this results in a large volume-averaged magnetic anisotropy energy, as large as 10^7 erg/cm³ [9], which is strongly dependent upon the parameters used in processing [10–12]. Empirical relationships between the magnetic anisotropy energy and the deposition temperature [19,20], working gas pressure [21], and stress [6], have been investigated in a-TbFe films. Cheng *et al.* [6] showed that the stress state of the film was responsible for only a fraction of the magnetic anisotropy. Kobayashi *et al.* [19] established the deposition temperature dependence of the uniaxial magnetic anisotropy constant, while Hellman and Gyorgy [20] showed that this enhancement is not strongly influenced by the stress state of the film nor due to surface dipoles as suggested by the work of Fu *et al.* [22].

In all sputter-deposition techniques, including the rf magnetron method used here, an energetic ion flux is incident upon a target material. Depending upon the ion's energy, mass, and trajectory, the incident ion may be buried within the surface of the target; cause structural rearrangements at the target surface; be reflected from the target surface retaining its kinetic energy; or impact the target, experience one or more elastic collisions, and cause the ejection of one or more neutral atoms from the surface (i.e., *sputtering*) [23]. Of the assortment of particles incident upon the substrate, the flux of working gas (i.e., Ar) ions and neutrals dominates and may contain particles having sufficient energy to resputter surface adatoms from the growing film.

In order to explore the effect of the Ar ion/neutral flux on a growing film, a series of Tb_{18.6}Fe_{81.4} films were processed using rf magnetron sputter deposition. The rf power and Ar gas pressure employed in processing were varied from 250–1000 W and 3.8–22.5 mTorr, respectively. The uniaxial magnetic anisotropy energy was determined

using the relationship $K_u = (1/2)MH_a$ and corrected for demagnetizing energy. The anisotropy fields (H_a) were determined by extrapolation of the linear portion of the magnetization (M) versus applied field curve in its approach to the saturation limit [1].

Table I lists the likely adatom arrangements for the case of the $\text{Tb}_{18.6}\text{Fe}_{81.4}$ films with their estimated binding [24] and threshold [25] energies for resputtering. Examination of the threshold energies indicates that an Ar ion/neutral incident at the film surface will sputter a surface adatom without a selective character if its energy is in excess of 65 eV. Correspondingly, if the Ar ion/neutral has an energy less than 34 eV, the energy communicated via an elastic collision to the adatom is insufficient to overcome the surface work function and no resputtering takes place. However, if the energy falls between these values, i.e., $34 \text{ eV} \leq E_{\text{Ar}} \leq 65 \text{ eV}$, then some adatoms are *selectively* resputtered from the surface of the growing film. By inspection of the threshold energies in Table I, ions having energies less than 56 eV favor the preferential removal of Fe adatoms of arrangements III, IV, and V leading to a greater number of Fe-Fe and Tb-Tb pairs along the film plane direction. It is noteworthy that this preference for like neighbor pairs parallel to the film plane is similar to that proposed by Gambino *et al.* [11] in 1973, and measured by Harris *et al.* [17] in 1992.

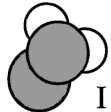
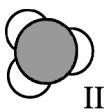



One difficulty in determining the probability and nature of selective resputtering is knowledge of the energy distribution of the Ar flux incident upon the growing film. In this regard, we have benefited from the work of Toups and Ernie [26], who measured the energy distribution of the Ar flux bombarding an electrode in a parallel plate rf reactor. Because their experiment resembles the geometry and conditions used here, their results have been extended to these studies. Figure 1 is a plot of the ion energy versus working gas pressure as a function of rf power. The solid symbols of Fig. 1 are derived from Ref. [26] and represent the measured energy of a distribution having a profile similar to that depicted in inset A. The ion energy that is expected to produce the most selective resputtering events and lead to the largest POA, as deduced from Table I, is denoted by the shaded bar in Fig. 1. This energy is determined by the distribution of ion energies in the plasma that is measured to have a sharp cutoff at high energies and a long tail at low energies (see inset A of Fig. 1). Increasing rf power with a fixed Ar pressure of ~ 7 mTorr shifts the

ion energy distribution away from the condition of maximum selective resputtering to a condition of nonselective resputtering. As is seen in inset B of Fig. 1, this acts to decrease the magnetic anisotropy energy. Correspondingly, the magnetic anisotropy increases with increasing gas pressure then rolls over at ~ 11 mTorr. This rollover is due to the increase in thermalizing collisions experienced by the Ar ions/neutrals in the plasma, which acts to decrease the number of Ar ions/neutrals that possess sufficient energy to resputter at the film surface. In this later curve, our data are plotted with the data of Kavalerov *et al.* [21], who previously measured the working gas-pressure dependence of magnetic anisotropy in rf magnetron-sputtered a-TbFe, and reported a similar behavior.

In order to determine the sputtering conditions that lead to a POA in these films, the anisotropic atomic structure was measured using EXAFS and correlated with the magnetic anisotropy and growth conditions. The x-ray absorption coefficient was measured over a photon energy range encompassing the Fe K (7112 eV) and Tb L_{III} (7514 eV) absorption edges for samples grown with varying rf power and Ar gas pressure. Data were collected [27] using normal and glancing angle (i.e., 10° with respect to the film plane) incident radiation, allowing for the sampling of in-plane and out-of-plane structure by aligning the electric field vector (\mathbf{E}) parallel and perpendicular to the film plane, respectively.

EXAFS analysis procedures followed those outlined in Ref. [28], resulting in the Fourier transformation of the extended fine structure to a radial coordinate. Fourier transformed (FT) Fe EXAFS data collected using normal and glancing incident radiation are presented in Fig. 2 for samples grown with varying rf power. The ASA that exists between data sets, primarily seen in the near neighbor (NN) peak centered near 2 \AA [29], is shown in an expanded view in the inset panels ($2a' - 2c'$). In the modeling analysis of the FT EXAFS data, theoretical data were generated using the FEFF-6 codes of Rehr *et al.* [15] and refined by fitting to a pure phase standard of TbFe_2 . The refined FEFF data were then fit to the phase and amplitude of the Fourier-filtered (FF) data in photoelectron wave vector (k) space via a parametrized nonlinear least squares method similar to that used in Ref. [17]. The modeling of the NN peak defines the coordination sphere around the Fe atoms to include contributions from 8.5 ± 0.7 Fe atoms centered near $2.49 \pm 0.02 \text{ \AA}$, and 1.4 ± 1 Tb atoms centered near

TABLE I. Adatom arrangements with binding energies and threshold energies defining selective resputtering conditions for a- $\text{Tb}_{19}\text{Fe}_{81}$ films. Adatom arrangements are depicted in top view where the large spheres represent Tb atoms and the small spheres represent Fe atoms.

Adatom arrangement	 I	 II	 III	 IV	 V
Binding energy (eV) [24]	13	15	14	13	12
Threshold energy (eV) [25]	56	65	40	37	34

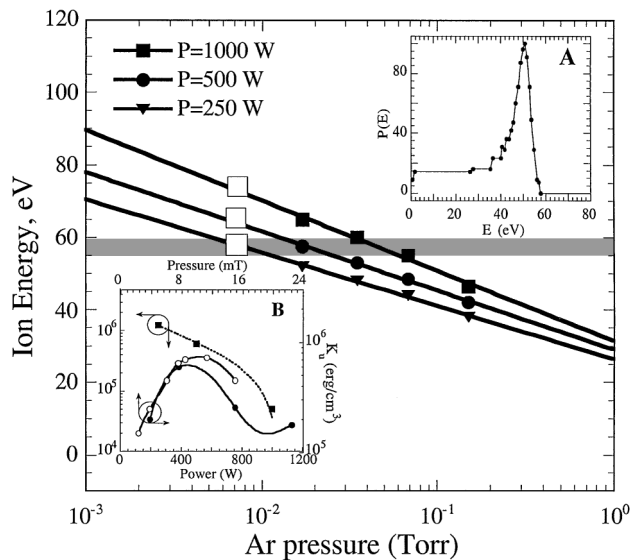


FIG. 1. Ion energies versus working gas pressure as a function of rf power. The measured energy distribution corresponding to an rf power of 250 W and an Ar pressure of 17 mT [26] is presented in inset (A) as representative of the energy distribution profile. Magnetic anisotropy energy (as K_u) is plotted as a function of rf power (at 7.6 mTorr) and working gas pressure (at 500 W) in inset (B). The solid symbols of inset (B) represent our data, and the hollow symbols are from Ref. [21].

$3.00 \pm 0.02 \text{ \AA}$. The structural anisotropy is quantified by modeling of the difference spectrum defined by subtracting the out-of-plane structure from the in-plane structure. These data directly reflect the structural anisotropy between the in-plane and out-of-plane atomic environments. A representative fit is illustrated in Fig. 3 for the sample whose FT EXAFS data are presented in Fig. 2a. The results of this fitting analysis are presented in Fig. 4 as a POA metric, specifically, as the percent change in the number of Fe-Fe pairs between the in-plane and out-of-plane environments. Although the anisotropy of the Tb environment is more strongly correlated to the PMA, direct measurement of this is difficult due to the few Tb ions surrounding the Fe ions, and the poorer signal to noise encountered in measuring the Tb L_{III} absorption edge. Nonetheless, the anisotropy around the Fe ions serves as an indirect measure of anisotropy around the Tb ions.

In Fig. 4, the measured PMA is plotted against the POA as a function of Ar ion energy in the plasma. A strong positive correlation exists between the PMA and the POA for Ar energies within the calculated resputtering energy envelope. Specifically, higher values of PMA and POA correspond with lower Ar energies determined previously to result in the preferential removal of Fe adatoms of arrangements III, IV, and V of Table I leading to a greater number of Fe-Fe and Tb-Tb pairs along the film plane direction. The projection of this curve onto the three two-dimensional planes indicates an exponential relationship between PMA and POA and Ar E, and a linear relationship between Ar E and POA. All films are presumed to be in the state of tension, as suggested by the work of Thornton

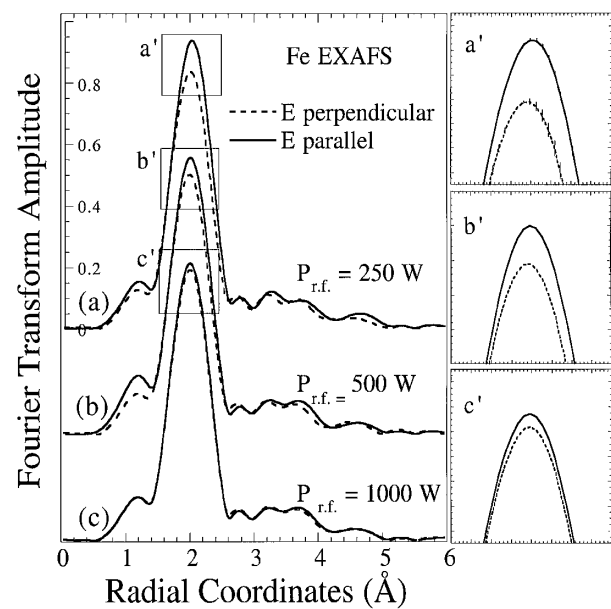


FIG. 2. Fourier transformed Fe EXAFS data for samples grown with increasing rf power. E is the electric vector of the incident radiation and identifies the direction along which the structure is sampled with a \cos^2 weighting. The atomic structural anisotropy is most evident in the near neighbor amplitude [see expanded insets (a), (b), and (c)]. A k range of $2.1-9.8 \text{ \AA}^{-1}$ with a k^2 weighting was applied during the Fourier transformation. The k -space range is truncated at 9.8 \AA^{-1} due to the onset of the Tb L_{III} absorption edge. Representative error bars are plotted on the data of inset (a').

[30]. Because the magnetostrictive coefficient for amorphous TbFe is positive [31], magnetoelastic interactions are not expected to increase PMA unless the films experience a compressive in-plane stress. For the sample having the smallest magnetic anisotropy energy, a POA that is beyond the detection limits of EXAFS, or dipole-dipole interactions as described earlier, may be responsible.

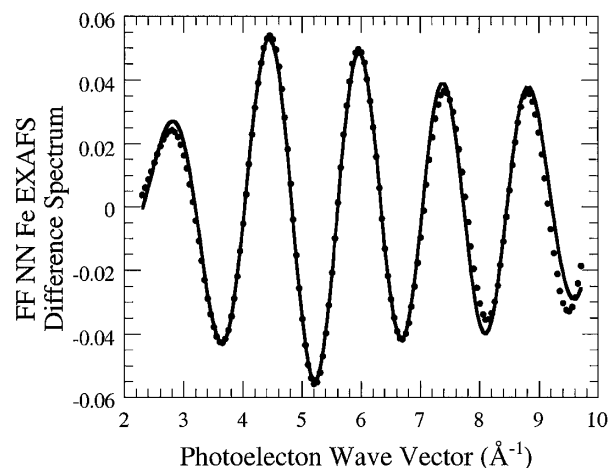


FIG. 3. Fourier-filtered (FF) near neighbor (NN) Fe EXAFS difference spectrum (as symbols) for the sample grown using 250 W and 7.6 mTorr Ar gas. The best fit, determined using a nonlinear least squares fitting of FEFF data, is shown as the solid curve.

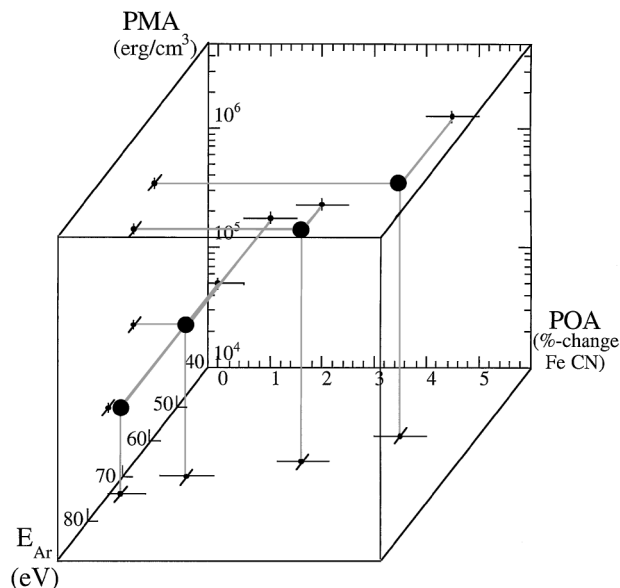


FIG. 4. Magnetic anisotropy energy plotted as PMA against the POA metric, percent change in the Fe-Fe coordination between the in-plane and perpendicular structure, and the Ar energy (E_{Ar}) of the plasma.

The measured POA directly reflects the anisotropic electrostatic field acting on the aspherical charge density of the Tb ion's $4f$ shell. This interaction leads to PMA from the rare earth single ion anisotropy, where the interaction energy depends on the orientation of the $4f$ magnetic moment. The rotation of this moment causes the rotation of the $4f$ charge cloud via a spin-orbit interaction. Self-consistent band structure calculations of electric field gradients in RE-TM intermetallic compounds by Coehoorn [32] indicate that the asphericity of the valence electron charge density on the RE ion provides the dominant contribution to the lowest order crystal field parameter (A_2^0), which in turn is proportional to the first order anisotropy constant (K_1). Our findings are consistent with the trends in magnetic anisotropy calculated by Coehoorn who found that the magnetic anisotropy was largest along the direction normal to the RE planes for REs having negative values for the second order Stevens coefficients (α_j) (e.g., Tb).

In summary, the PMA in rf magnetron sputtered a-TbFe films is shown to increase exponentially with POA induced by the selective resputtering of surface adatoms during film growth. After nearly three decades of experimental and theoretical research, both the source of PMA and the mechanism by which it is incorporated in sputtered a-RETM films are now understood.

The authors thank Dr. Kristl Hathaway and Dr. Tim Elam for helpful comments in the preparation of this manuscript. This research was supported by the Office of Naval Research.

[1] S. Chikazumi and S.H. Charap, *Physics of Magnetism* (John Wiley & Sons, Inc., New York, 1964).

- [2] G.S. Cargill and T. Mizoguchi, *J. Appl. Phys.* **49**, 1753–1755 (1978).
- [3] S. Esho and S. Fujiwara, in *Magnetism and Magnetic Materials*, AIP Conf. Proc. No. 34 (AIP, New York, 1976), p. 331.
- [4] P.W. Rooney *et al.*, *Phys. Rev. Lett.* **75**, 1843 (1995).
- [5] D. Weller *et al.*, *J. Magn. Magn. Mater.* **121**, 461 (1998).
- [6] S.C.N. Cheng *et al.*, *IEEE Trans. Magn.* **25**, 4018–4020 (1989).
- [7] R. Naik *et al.*, *Phys. Rev. B* **51**, 3549 (1995).
- [8] J.H. van Vleck, *Phys. Rev.* **52**, 1178 (1937).
- [9] F. Hellman *et al.*, *Phys. Rev. B* **39**, 10591–10605 (1989).
- [10] T. Mizoguchi and G.S. Cargill, *J. Appl. Phys.* **50**, 3570–3582 (1979).
- [11] R.J. Gambino *et al.*, in *Magnetism and Magnetic Materials*, AIP Conf. Proc. No. 18 (AIP, New York, 1973), pp. 578–592.
- [12] P. Chaudhari *et al.*, *Appl. Phys. Lett.* **22**, 337–339 (1973).
- [13] R.J. Gambino and J.J. Cuomo, *J. Vac. Sci. Technol.* **15**, 296–301 (1978).
- [14] J.J. Rehr *et al.*, *J. Am. Chem. Soc.* **113**, 5135 (1991).
- [15] J.J. Rehr *et al.*, *Phys. Rev. Lett.* **69**, 3397 (1992).
- [16] A. Erbil *et al.*, *Phys. Rev. B* **37**, 2450 (1988).
- [17] V.G. Harris *et al.*, *Phys. Rev. Lett.* **69**, 1939 (1992); V.G. Harris *et al.*, *Phys. Rev. B* **49**, R3637 (1994).
- [18] S.S. Jaswal, *Phys. Rev. Lett.* **68**, 1440 (1992).
- [19] H. Kobayashi *et al.*, *Appl. Phys. Lett.* **43**, 389–390 (1983).
- [20] F. Hellman and E.M. Gyorgy, *Phys. Rev. Lett.* **68**, 1391–1394 (1992).
- [21] V.G. Kavalero *et al.*, *IEEE Trans. Magn.* **29**, 3111 (1993).
- [22] H. Fu *et al.*, *Phys. Rev. Lett.* **66**, 1086 (1991).
- [23] B. Chapman, *Glow Discharge Processes: Sputtering and Plasma Etching* (John Wiley & Sons, Inc., New York, 1980).
- [24] The binding energies were estimated using values applied by Gambino and Cuomo in Ref. [13] assuming that the adatoms bond in a milk-stool geometry forming tetrahedrons.
- [25] The threshold energies were calculated by applying the laws of conservation of energy and momentum to a two-elastic collision process in a single knock-on regime.
- [26] M.F. Toups and D.W. Ernie, *J. Appl. Phys.* **68**, 6125 (1990); M.F. Toups, Ph.D. thesis, University of Minnesota, 1985.
- [27] Data collection was performed using a total electron yield technique at beam line X23B at the National Synchrotron Light Source (Brookhaven National Laboratory, Upton, NY). At the time data were collected the storage ring energy was 2.54 GeV and the ring current ranged from 180–250 mA.
- [28] D.E. Sayers and B.A. Bunker, in *X-ray Absorption: Principles, Applications, Techniques of EXAFS, SEXAFS, and XANES*, edited by D.C. Koningsberger and R. Prins (John Wiley & Sons, New York, 1988), Vol. 92, pp. 211–253.
- [29] Electron phase shifts have not been corrected for at this stage in the analysis, and therefore the Fourier transform peak positions do not reflect true radial distances but are shifted to lower r values.
- [30] J.A. Thornton and D.W. Hoffman, *Thin Solid Films* **171**, 5 (1989).
- [31] A.E. Clark, in *Ferromagnetic Materials*, edited by E.P. Wohlfarth (North-Holland Publishing Co., Amsterdam, 1980), Vol. 1, pp. 531–589.
- [32] R. Coehoorn, *J. Magn. Magn. Mater.* **99**, 55 (1991).